Flow Field and Oscillation Frequency of a Rotating Liquid Droplet

TADASHI WATANABE
Center for Computational Science and e-Systems
Japan Atomic Energy Agency (JAEA)
Tokai-mura, Naka-gun, Ibaraki-ken, 319-1195
JAPAN
watanabe.tadashi66@jaea.go.jp http://www.jaea.go.jp

Abstract: - Oscillations and rotations of a liquid droplet are simulated numerically using the level set method, and the combined effects of oscillation amplitude and rotation rate on the drop-shape oscillation is studied. The oscillation frequency is shown to decrease as the amplitude of oscillation increases. The oscillation frequency increases, in contrast to the effect of amplitude, as the rotation rate increases. The pressure distribution in the droplet corresponds to the frequency shift, and it is shown that the oscillations without frequency shift are possible. It is found that the relation between the amplitude and the rotation rate is linear both for the frequency shift of zero and for the pressure difference of zero even though the fluid properties are different. The flow fields in and around the droplet are visualized, and it is shown that the vortices formed by the oscillation are not affected by the rotation. Parallel computations are performed with satisfactory high efficiency for the calculations of the pressure field, and the importance of the communication rate is demonstrated.

Key-Words: - Droplet, Oscillation, Amplitude, Rotation, Frequency, Level Set Method, Parallel Computation

1 Introduction

A levitated liquid droplet is used to measure material properties of high temperature molten metal, since the levitated droplet is not in contact with a container, and the effect of the container wall is eliminated for a precise measurement. The levitation of liquid droplets, which is also used for containerless processing of material, is controlled by using electromagnetic force [1], electrostatic force [2], or acoustic force [3] under the gravitational condition. Viscosity and surface tension are, respectively, obtained from the damping and the frequency of drop-shape oscillations. The relation between material properties and oscillation parameters is based on the linear theory [4], and small amplitude oscillations are necessary. Large amplitude oscillations are, however, desirable from the viewpoint of measurement or experiment.

The oscillation frequency has been shown to decrease with increasing amplitude of the drop-shape oscillations experimentally by Trinh and Wang [5]. The decrease in oscillation frequency has been calculated for moderate amplitude axisymmetric oscillations of incompressible inviscid drops by Tsamopoulos and Brown [6]. The calculated results were in qualitative agreement with the experimental results. The effect of amplitude on the oscillation frequency has been discussed theoretically by Azuma and Yoshihara [7]. Second order small deviations were taken into account for the linearized solution, and the oscillation frequency was shown to decrease as the amplitude increased. The effect of rotation, on the other hand, has been discussed by Busse [8] and Lee et al. [9] theoretically, and by Wang et al. [10] experimentally. In contrast to the effect of amplitude, the oscillation frequency increased by rotation. Although effects of amplitude and rotation were shown in these studies, the relation between the frequency shift and the flow field in the droplet has not been considered well.

In this study, numerical simulations of an oscillating-rotating liquid droplet are performed to study the effects of amplitude and rotation on the oscillation frequency. Three-dimensional Navier-Stokes equations are solved using the level set method [11]. In this method, the level set function, which is the distance function from the droplet surface, is calculated by solving the transport equation to obtain the position of the surface correctly. Mass conservation of the droplet is especially taken into account in the calculation of the level set function. The staggered mesh system is used and the second-order upwind difference scheme is applied for convective terms. The second-order Adams-Bashforth method is used for time integration. Parallel computations are performed by applying domain decomposition technique. The oscillation of the rotating droplet is simulated by

changing the amplitude and the rotation rate, and the combined effects of amplitude and rotation on the oscillation frequency and the flow field in and around the droplet are studied. The relation between the frequency and the flow field is discussed in terms of the pressure distribution in the droplet.

2 Numerical Simulations

2.1 Governing equations

The level set method [11] is outlined briefly in the following. Governing equations for the droplet motion are the equation of continuity,

$$\nabla \cdot u = 0, \tag{1}$$

and the incompressible Navier-Stokes equations,

$$\rho \frac{Du}{Dt} = -\nabla p + \nabla \cdot (2\mu D) - F_s, \tag{2}$$

where ρ, u, p and μ, respectively, are the density, the velocity, the pressure and the viscosity, D is the viscous stress tensor, and F_s is a body force due to the surface tension. The surface tension force is given by

$$F_s = \sigma \kappa \delta \nabla \phi, \tag{3}$$

where σ, κ, δ and ϕ are the surface tension, the curvature of the interface, the Dirac delta function and the level set function, respectively. The level set function, which is the normal distance from the interface, is defined as $\phi=0$ at the interface, $\phi<0$ in the liquid region, and $\phi>0$ in the gas region. The curvature is expressed in terms of ϕ:

$$\kappa = \nabla \cdot (\frac{\nabla \phi}{|\nabla \phi|}). \tag{4}$$

The density and viscosity are given by

$$\rho = \rho_l + (\rho_g - \rho_l) H, \tag{5}$$

and

$$\mu = \mu_l + (\mu_g - \mu_l) H, \tag{6}$$

where the subscripts g and l denote the gas and liquid phase, respectively, and H is a Heaviside-like function defined by

$$H = \begin{cases} 0 & (\phi < -\varepsilon) \\ \frac{1}{2}[1 + \frac{\phi}{\varepsilon} + \frac{1}{\pi}\sin(\frac{\pi\phi}{\varepsilon})] & (-\varepsilon \le \phi \le \varepsilon), \\ 1 & (\varepsilon < \phi), \end{cases} \tag{7}$$

where ε is a small positive constant for which $|\nabla \phi| = 1$ for $|\phi| \le \varepsilon$. The evolution of ϕ is given by

$$\frac{\partial \phi}{\partial t} + u \cdot \nabla \phi = 0. \tag{8}$$

In order to maintain the level set function as a distance function, an additional equation is solved:

$$\frac{\partial \phi}{\partial \tau} = (1 - |\nabla \phi|) \frac{\phi}{\sqrt{\phi^2 + \alpha^2}}, \tag{9}$$

where τ and α are an artificial time and a small constant, respectively. The level set function becomes a distance function in the steady-state solution of the above equation. The following equation is also solved to preserve the total mass in time [12]:

$$\frac{\partial \phi}{\partial \tau} = (A_o - A)(1 - \kappa)|\nabla \phi|, \tag{10}$$

where A_0 denotes the total mass for the initial condition and A denotes the total mass corresponding to the level set function. The total mass is conserved in the steady-state solution of the above equation.

All variables are nondimensionalized using liquid properties and characteristic values: $x'=x/L$, $u'=u/U$, $t'=t/(L/U)$, $p'=p/(\rho_l U^2)$, $\rho'=\rho/\rho_l$, $\mu'=\mu/\mu_l$, where the primes denote dimensionless variables, and L and U are representative length and velocity, respectively. The representative length and velocity may be the droplet diameter and the velocity of the surface, respectively. In the following numerical simulations, however, two non-dimensional numbers, the Reynolds number, $\rho_l LU/\mu_l$, and the Weber number, $\rho_l LU^2/\sigma$, are only necessary.

2.2 Numerical conditions

Shape oscillations of a rotating droplet, whose rotation axis is vertical and the same as the oscillation axis, are simulated in the following.

The finite difference method is used to solve the governing equations. The staggered mesh system is applied for spatial discretization of velocities. The convective terms are discretized using the second order upwind scheme and other terms by the central difference scheme. Time integration is performed by the second order Adams-Bashforth method. The SMAC method [13] is used to obtain pressure and velocities. The Poisson equation for pressure correction is solved using the Bi-CGSTAB method. The domain decomposition technique is applied and the message passing interface (MPI) library is used for parallel numerical simulations. The block Jacobi preconditioner [14] is used and the simulations are performed with the parallel computer systems in JAEA: SGI Altix3700, Altix350, and some PC clusters.

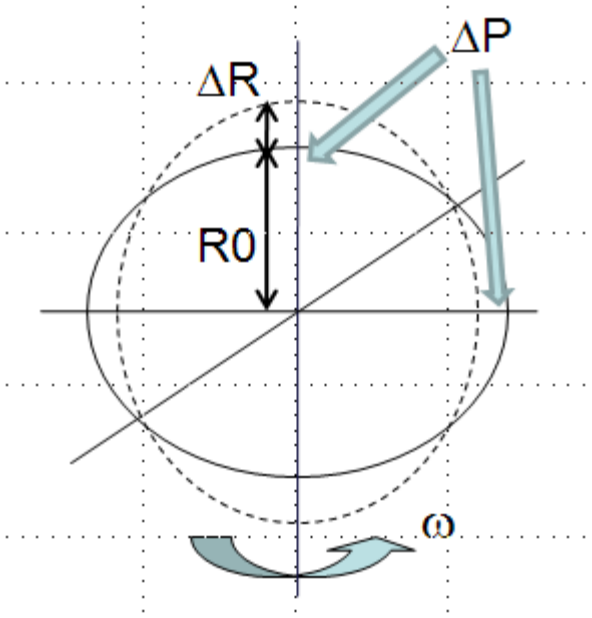

Fig. 1 Schematic of oscillating-rotating droplet.

The effects of region size and noding on simulation results have been examined beforehand for the average droplet radius of unity. The number of calculation nodes in three-dimensional space was determined to be 100x100x100 ~ 140x140x140 so as to eliminate the size effect. The spatial increment was 0.03 in all directions, and the size of the simulation region was thus 3.0x3.0x3.0 ~ 4.2x4.2x4.2. Periodic boundary conditions are applied at all the boundaries of the simulation region. Figure 1 shows the schematic of an oscillating-rotating liquid droplet. An ellipsoidal droplet is placed at the centre of the simulation region, and the initial rotation is imposed as a rigid rotation with a constant angular velocity, ω, around the vertical axis. The initial amplitude, ΔR, in the vertical direction is given as a normalized deformation from the average shape of the rotating droplet. The average vertical radius, R0, is determined from the rotation of a spherical droplet. The density ratio and the viscosity ratio are both fixed at 0.01. The time step size is determined so as to satisfy the CFL conditions [15].

In the nondimensional form of the governing equations, the Reynolds number and the Weber number are varied from 200 to 400 and from 10 to 30, respectively, in the following simulations. The initial amplitude is varied from 0.02 to 0.83. The rotation rate, which is normalized by the oscillation frequency for the non-rotating droplet with the amplitude of 0.02, is varied from 0.0 to 0.6.

Calculated oscillation periods using the present method for a droplet without rotation have been compared with the theoretical values for validation [16]. The calculated periods for oscillation mode 2, 3 and 4 were 10.1, 5.23 and 3.40, respectively, while the theoretical values were 10.0, 5.15 and 3.32. It was also reported for small rotation rates that the calculated frequencies using the present method were in good agreement with the theoretical result [16].

3 Results and Discussions

3.1 Velocity fields

Variations of droplet shape and velocity fields over the first oscillation period are shown in Figs. 2 and 3 as examples of an oscillating-rotating liquid droplet. The vertical cross section along the vertical axis in Fig. 1 is shown in Fig. 2, and the horizontal cross section along the horizontal axes is shown in Fig. 3. The rotation rate is 0.3 and the initial amplitude is 0.38. The Reynolds number and the Weber number are 200 and 20, respectively.

The initial prolate shape at T=0.0 becomes oblate shape gradually as shown in Fig. 2, and the internal flow is induced from the vertical top and bottom to the centre of the droplet and from the centre to the horizontal side direction as shown at T=2.31. The external flow field develops immediately according to the variation of the droplet shape. Four vortex centres are seen in the vertical cross section in between the pole and the equator. It indicates that two three-dimensional vortices appear around the droplet. The vertical radius is almost the smallest at T=4.61, and the droplet shape is oblate. The flow reversal is clearly seen at T=6.92. The vertical radius becomes large at T=9.23, and the droplet shape is prolate again. The next oscillation period starts, and the flow direction is reversed again at T=11.53. The shape oscillation continues around the

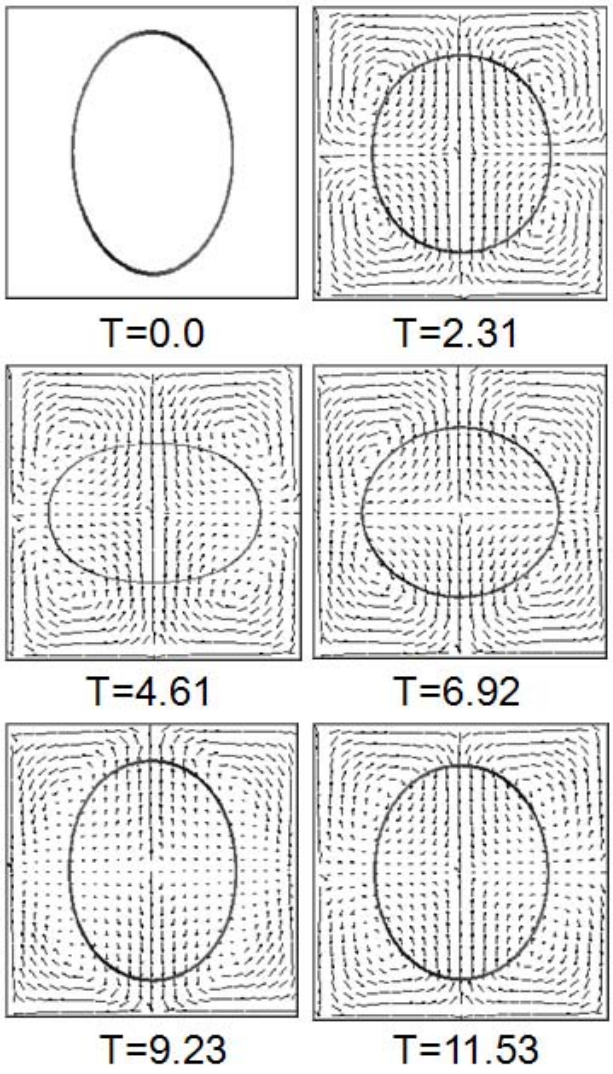

Fig.2 Velocity field in vertical cross section.

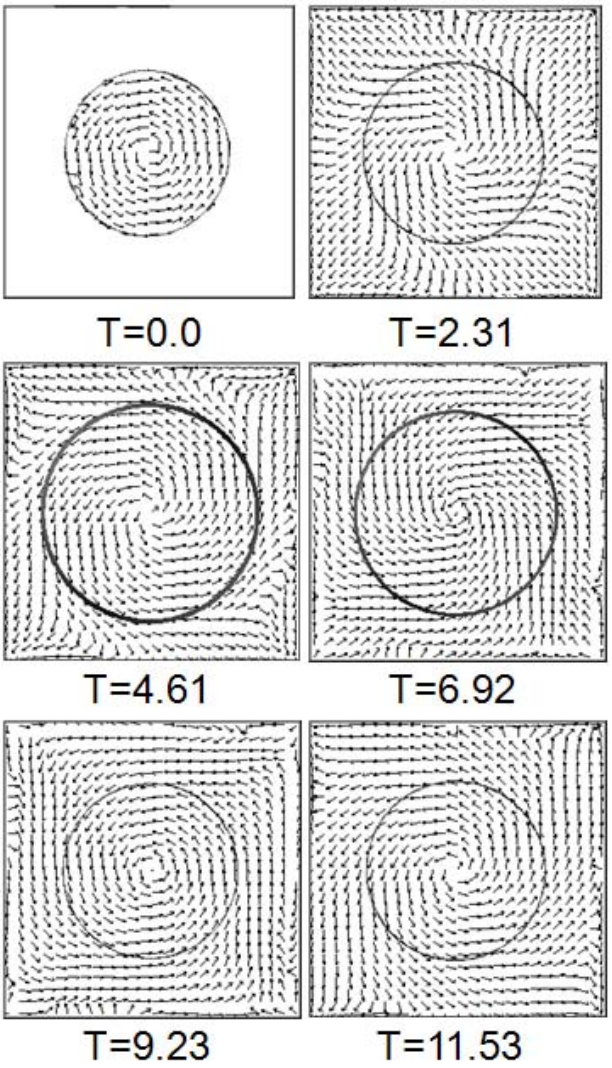

Fig.3 Velocity field in horizontal cross section.

equilibrium shape of the rotating droplet. The velocity fields in and around the droplet are similar to those for a non-rotating droplet [16], and it is found that the vertical velocity fields are not affected much by rotation.

The rotating velocity field in the horizontal cross section is shown in Fig. 3. The rotation rate is imposed as a rigid rotation at T=0.0. The initial rotation is applied only in the droplet as shown in Fig. 3. The external flow field, however, develops immediately in the horizontal direction. The flow direction is counter clockwise in this example. The outward flow is seen at T=2.31, since the droplet shape is varying from prolate to oblate. The horizontal cross section of the droplet becomes the largest at T=4.61, and the velocity at the interface is almost tangential. The inward flow is seen at T=6.92, and the horizontal cross section becomes the smallest at T=9.23. The droplet shape is oblate at T=4.61, and prolate at T=9.23 as shown in Fig. 2. Vortices do not appear around the droplet in the horizontal cross section.

3.2 Vortex fields

Vortex fields around the droplet at several time levels are shown in Figs. 4 and 5. The surface with the vorticity of 0.03 is visualized. The vortex fields corresponding to the oscillating-rotating droplet in Figs. 2 and 3 are shown in Fig. 4, while the vortex fields for a non-rotating droplet are shown in Fig. 5 for comparison. The initial amplitude is 0.38 in Figs. 4 and 5, and the rotation rate is 0.3 in Fig. 4. The equilibrium shape is an ellipsoid for the rotating droplet, while it is a sphere for the non-rotating

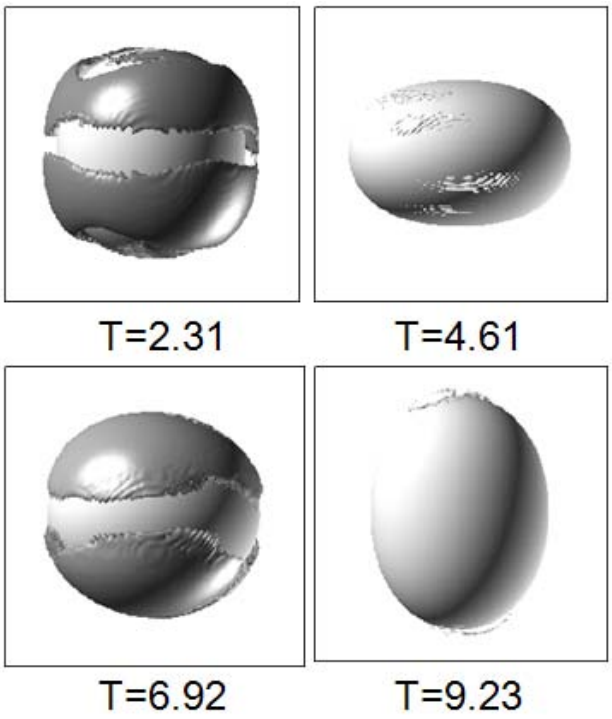

Fig.4 Vortex field around rotating droplet.

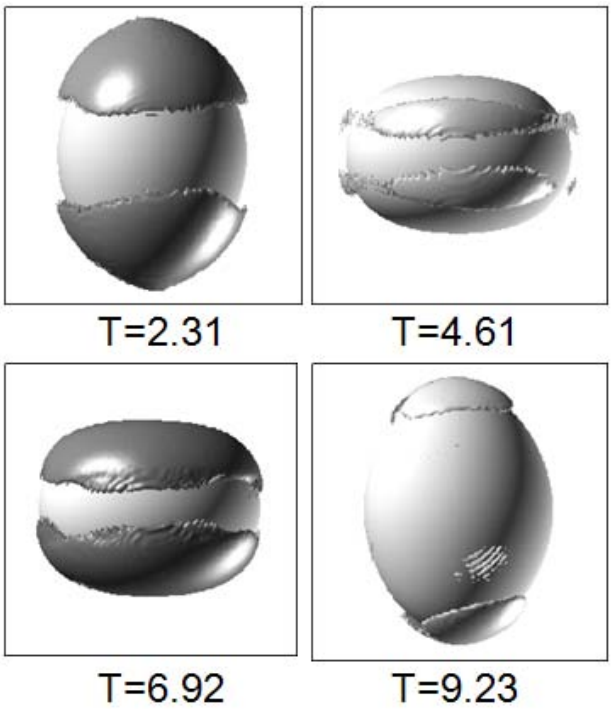

Fig.5 Vortex field around non-rotating droplet.

droplet, and the droplet shape is slightly different as shown in Figs. 4 and 5.

Two large vortices are seen clearly at T=2.31 and 6.92 in Fig. 4, while vortices almost vanish at

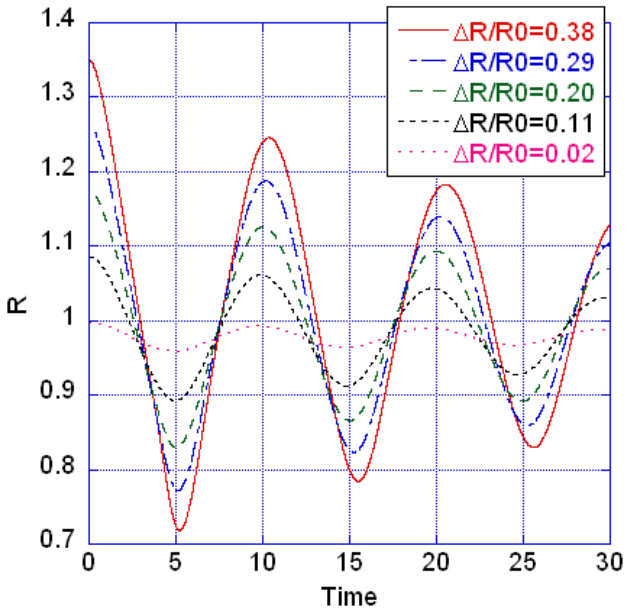

Fig.6 Effect of amplitude on time history of droplet radius: ω=0.2.

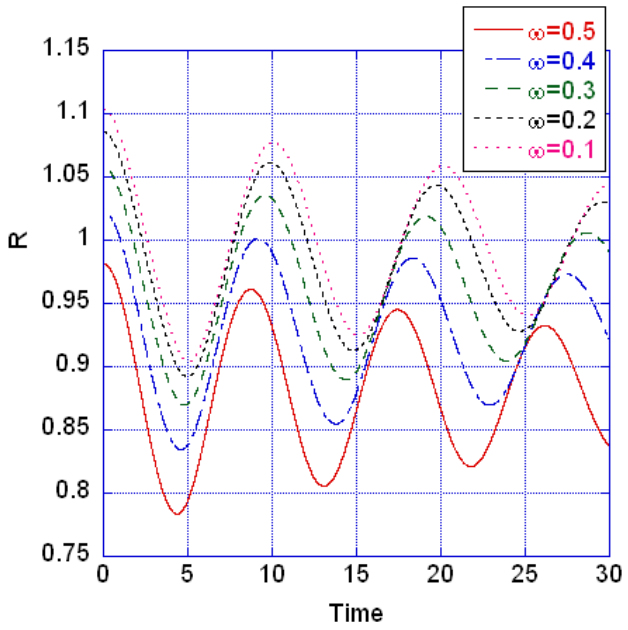

Fig.7 Effect of rotation rate on time history of droplet radius: ΔR/R0=0.11.

T=4.61 and 9.23. It is found that large or strong vortices appear when the droplet shape is varying between prolate and oblate. Large vortices correspond to large velocities around the droplet as shown in Fig. 2. The vortex fields for the non-rotating droplet in Fig. 5 are similar to those for the oscillating-rotating droplet shown in Fig. 4, though the vortex size is slightly smaller for the oscillating-

rotating droplet. Vortices are seen clearly in the vertical velocity fields as shown in Fig. 2, and not in the horizontal velocity fields in Fig. 3. It is found in Figs. 4 and 5 that the vortex field is not much affected by the rotation.

3.3 Oscillation frequency

Time evolutions of the droplet radius, R, are shown in Figs. 6 and 7 for the case with the Reynolds number of 200 and the Weber number of 20. The droplet radius is defined as the distance between the top and the centre of the droplet: initially R0+ΔR in Fig. 1. The effect of amplitude is shown in Fig. 6, where five cases with different amplitude are shown. The rotation rate is 0.2. It is seen in Fig. 6 that the oscillation curves shift toward the positive direction of the time axis as the amplitude increases. It indicates the oscillation period becomes large as the amplitude increases. In other words, the oscillation frequency decreases as the amplitude increases. The effect of rotation is shown in Fig. 7, where five cases with different rotation rate are shown. The initial amplitude is 0.11. It is seen in Fig. 7 that the oscillation curves shift toward the negative direction of the time axis as the rotation rate increases. It means, in contrast to the effect of amplitude shown in Fig. 6, the oscillation period becomes small as the rotation rate increases. In other words, the oscillation frequency increases as the rotation rate increases. The decrease in frequency due to the increase in amplitude has been observed in the experiment for non-rotating droplets [5], and the increase in frequency due to the increase in rotation has also been observed [17].

The variation of oscillation frequency due to the change in amplitude and rotation rate is shown in Fig. 8 for the case with the Reynolds number of 200 and the Weber number of 20. The frequency shift indicates the frequency difference, ΔF, normalized by the oscillation frequency for the non-rotating droplet with the amplitude of 0.02, F0. In the linear theory, the oscillation frequency, ω, for the lowest mode of oscillation is a constant obtained in terms of the surface tension, the density, and the droplet

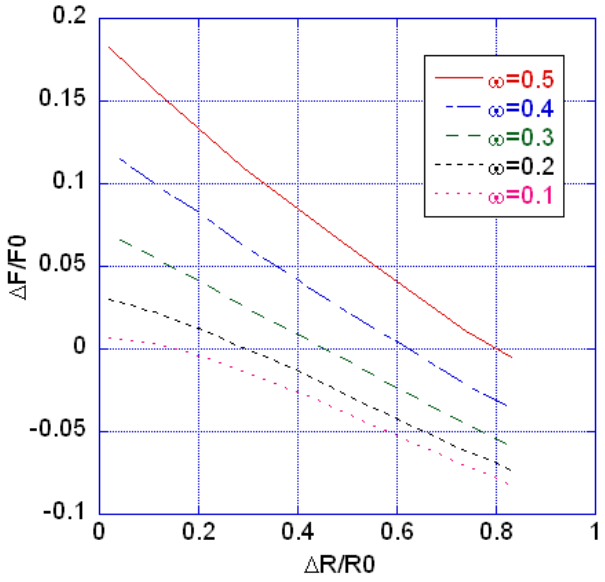

Fig.8 Effect of rotation rate on frequency shift.

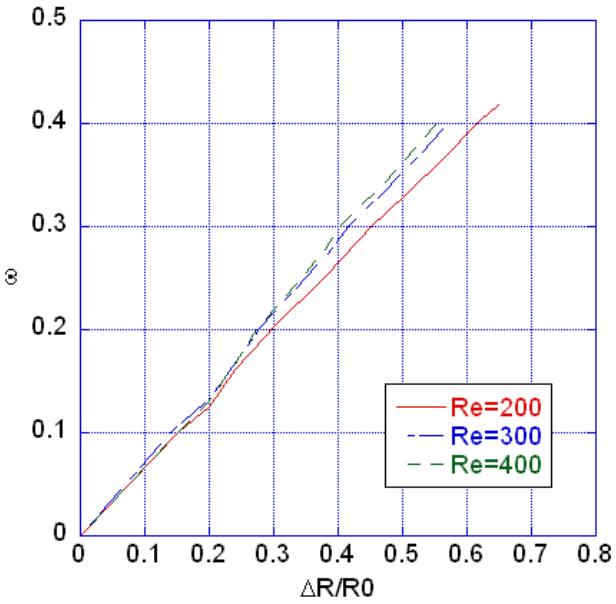

Fig.9 Condition for frequency shift of zero: effect of viscosity.

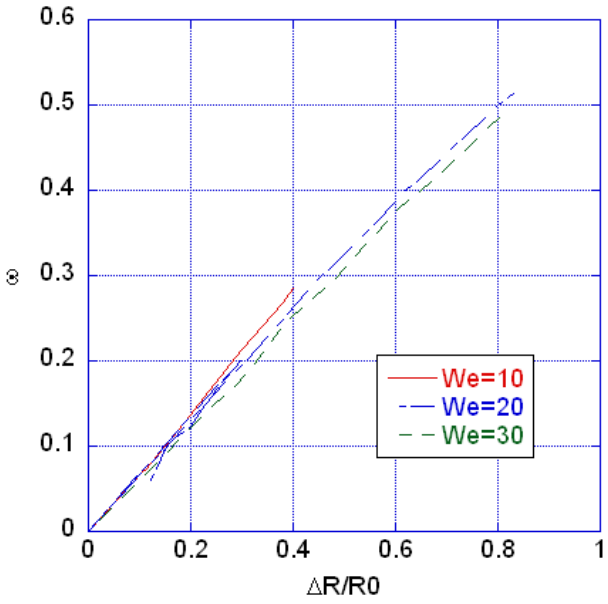

Fig.10 Condition for frequency shift of zero: effect of surface tension.

radius [4]:

$$\omega^2 = \frac{8\sigma}{\rho R^3} \ . \qquad (11)$$

The oscillation frequency is, however, shown to be affected largely by amplitude and rotation. This is important for experiments, since large oscillations are desirable for measurements and slight rotations are sometimes necessary for stability of oscillating droplets. It is shown clearly in Fig. 8 that the oscillation frequency decreases as the amplitude increases, while it increases as the rotation rate increases. Each curve with the different rotation rate is shown to cross the horizontal line with ΔF/F0=0. It is thus found that the oscillations without frequency shift are possible even for the cases with large amplitude by an appropriate combination between the amplitude and the rotation rate [18].

The relation between the amplitude and the rotation rate for the frequency shift of zero is shown in Figs. 9 and 10. Effects of viscosity and surface tension are shown by changing the Reynolds number and the Weber number, respectively. It is found that the conditions for the frequency shift of zero are represented by the linear relation between the amplitude and the rotation rate through the origin even though the fluid properties are different. The gradients of linear relation are, however, slightly affected by the viscosity and the surface tension.

3.4 Pressure fields

The oscillation of the droplet shape is induced by the force balance in the droplet, which is the pressure distribution corresponding to the difference of surface tension force due to the difference of surface curvature. The pressure difference in the droplet is thus closely related to the frequency shift.

The pressure distributions along the vertical and horizontal axes are shown in Figs. 11 and 12, respectively. The rotation rate is 0.2 and the initial amplitude is 0.29. The Reynolds number is 200 and the Weber number is 20. The average pressure in the droplet is about 0.1 in this case, since the pressure due to the surface tension is given by *2/We* in the non-dimensional form. The inside pressure is oscillating around the average pressure. The outside pressure is set equal to zero in our simulations. The pressure distribution is rather flat and the droplet radius is almost 1.0 at T=2.31 in Figs. 11 and 12. At T=4.61, however, it is seen in Fig. 11 that the polar pressure is low and the vertical radius is small. The equatorial pressure becomes high simultaneously and the horizontal radius is large as shown in Fig. 12. The droplet shape is oblate at this time and the surface curvature is large at the equator. The pressure distribution becomes rather flat again and the droplet shape becomes nearly a sphere at T=6.92. The droplet shape is prolate at T=9.23, and the polar pressure is high, while the equatorial pressure is low. The centre pressure is always in between the polar and equatorial pressures. It is seen in Figs. 11 and 12 that the pressure distribution in the droplet oscillates corresponding to the droplet shape.

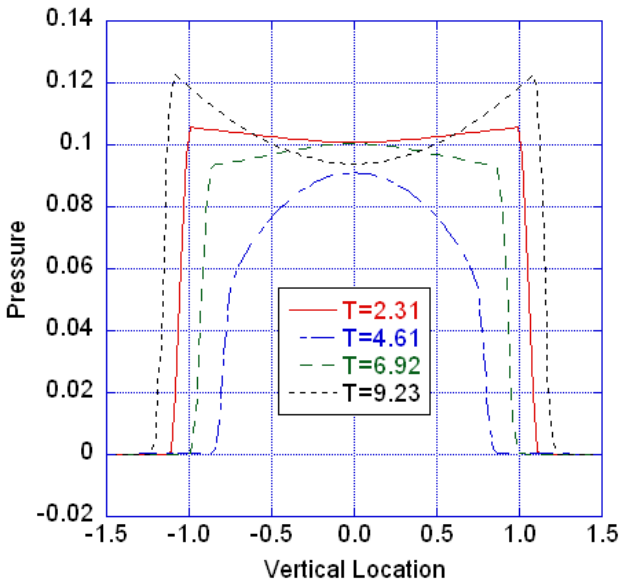

Fig.11 Vertical pressure distribution.

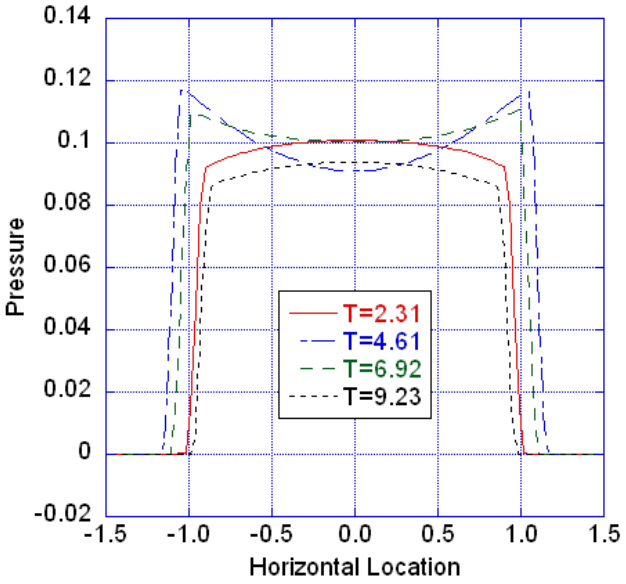

Fig.12 Horizontal pressure distribution.

3.5 Pressure difference

The variation of pressure difference in the droplet is shown in Figs. 13 and 14 corresponding to the variation of droplet radius shown in Figs. 6 and 7. The pressure difference, ΔP, is defined as the pressure difference between the vertical top (pole) and the horizontal side (equator) of the droplet as shown in Fig. 1. The pressure difference is positive when the droplet shape is prolate, while it is negative when the droplet shape is oblate. The time history of the pressure difference in Figs. 13 and 14 are, thus, similar to the evolution of the droplet radius shown in Figs. 6 and 7.

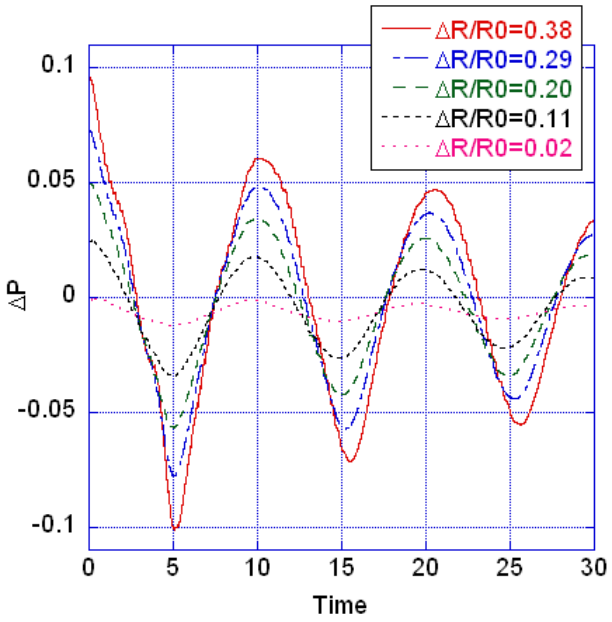

Fig.13 Effect of amplitude on time history of pressure difference: ω=0.2.

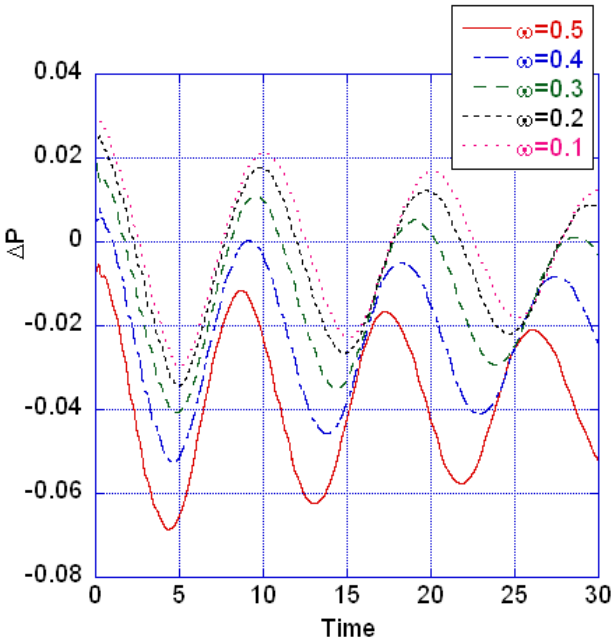

Fig.14 Effect of rotation rate on time history of pressure difference: ΔR/R0=0.11.

The variation of average pressure difference due to the change in amplitude and rotation rate is shown in Fig. 15 for the case with the Reynolds number of 200 and the Weber number of 20. It is found that the pressure difference has the opposite tendency to the frequency shift shown in Fig. 8. The pressure difference increases as the amplitude increases, and decreases as the rotation rate increases. The pressure at the top of the droplet becomes higher than that at the side as the amplitude increases, since the curvature and the surface tension force become larger at the top. The pressure difference thus increases as the amplitude increases. On the other hand, the pressure at the side of the droplet becomes higher than that at the top as the rotation rate increases, since the centrifugal force increases. The pressure difference thus decreases as the rotation rate increases. These effects are combined in the oscillating-rotating liquid droplets. It is found in Fig. 15 that each curve with the different rotation rate crosses the horizontal line with ΔP=0. The average flow fields without pressure difference are thus possible by imposing an appropriate rotation on oscillating droplets [16].

The relation between the amplitude and the

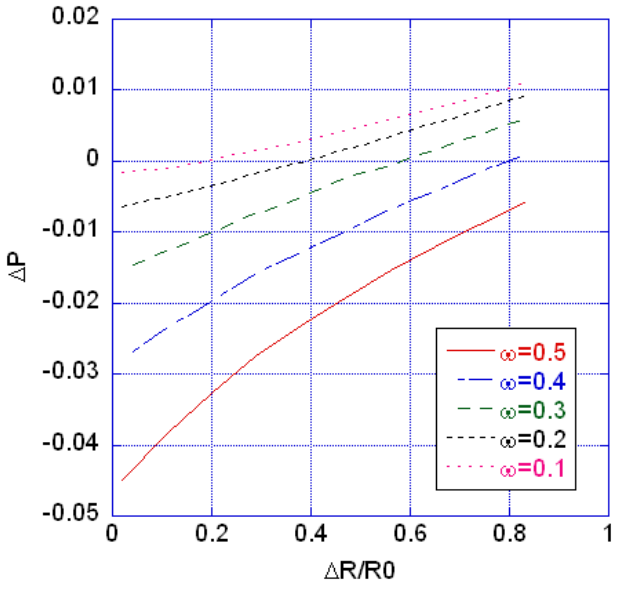

Fig.15 Effect of rotation rate on pressure difference.

rotation rate for the pressure difference of zero is shown in Figs. 16 and 17. The effects of viscosity and surface tension are indicated in terms of the Reynolds number and the Weber number, respectively. The condition for the pressure difference of zero is seen to be similar to that for the frequency shift of zero: the conditions for the pressure difference of zero are represented by the linear relation between the amplitude and the rotation rate through the origin even for different fluid properties. The gradient is, however, slightly affected by the fluid properties. It is confirmed in Figs. 16 and 17 that the pressure difference in the droplet corresponds to the frequency shift.

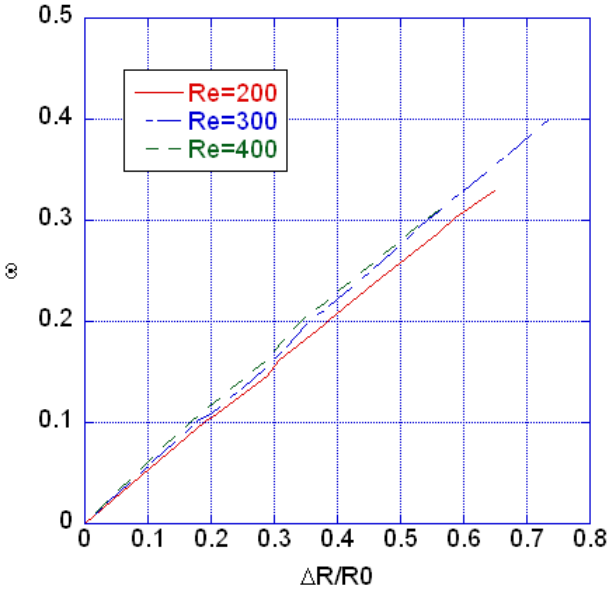

Fig.16 Condition for pressure difference of zero: effect of viscosity.

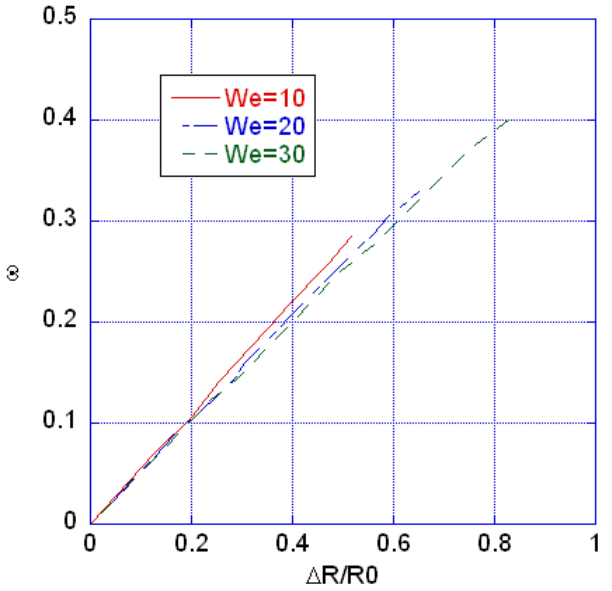

Fig.17 Condition for pressure difference of zero: effect of surface tension.

3.6 Parallel calculations

The incompressible Navier-Stokes equations are solved to obtain the flow fields in the above level set method. The pressure Poisson equations are calculated iteratively at each time step using the Bi-CGSTAB method. The parallel computations are applied to solve the Poisson equations, since this part is the most time consuming part in our simulations. The domain decomposition technique is applied and the message passing interface (MPI) libraries are used for parallelization.

The speed up of parallel numerical simulation is shown in Fig. 18. The total calculation time is indicated by 'Elapse Time', while the time for matrix calculations to solve the pressure Poison equations using the parallel Bi-CGSTAB method by 'Matrix Calculation Time'. Two parallel computer systems are compared in Fig. 18: Altix3700 and Altix350. Both the systems are made by SGI, and Intel Itanium2 processors are used with a clock rate of 1.6 GHz. It is shown for Altix3700 that the speed up of total calculation time is about 32 with 48 processors, and the speedup of matrix calculation time is about 48 with 48 processors. The parallel efficiency for the Bi-CGSTAB method is found to be satisfactory in our simulations. Altix350 shows the same tendency, but the speed up is slightly lower. This is due to the difference in communication rate. Altix3700 has 128 processors on a node, while Altix350 has 2. The inter node data communication is necessary for Altix350, and this affects the speed up as shown in Fig. 18. The effect of the inter node communication is small when the number of processors is smaller than 8.

The speed up for small scale parallel calculations is shown in Fig. 19. The results with a PC cluster, which is composed of AMD Athlon 3.4 GHz connected with 1 Gbps network, are shown along with the Altix350 results. It is shown in Fig. 19 that the speed up is largely affected by the communication rate. The inter node communication rate of Altix350 is 8 Gbps, and thus 8 times faster than the ordinary network for the PC cluster. It is also seen in Fig. 19 that the speed up decreases for the PC cluster when more than 5 processors are used. The total calculation time and the matrix calculation time using a single processor are 640.04 s and 573.85 s, respectively for Altix350, while 417.87 s and 363.39 s for the PC cluster. The calculation speed using a single processor is, thus, faster for the PC cluster. The iterative calculations are the most

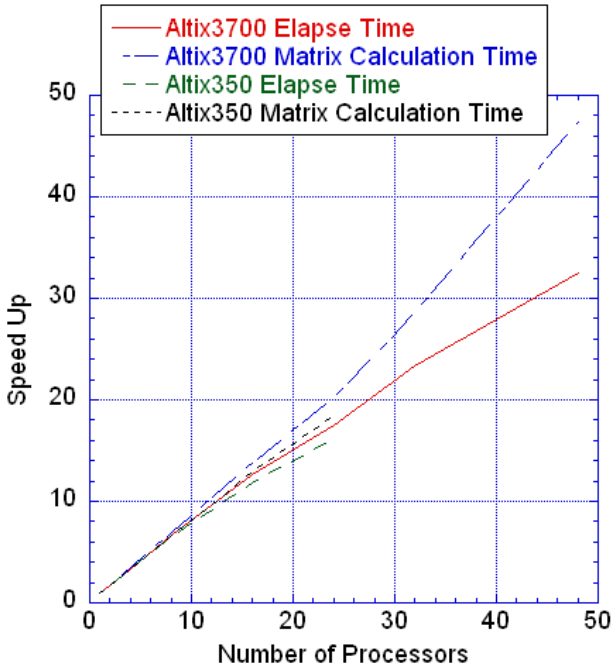

Fig.18 Speed up of parallel computations: comparison of parallel computer systems.

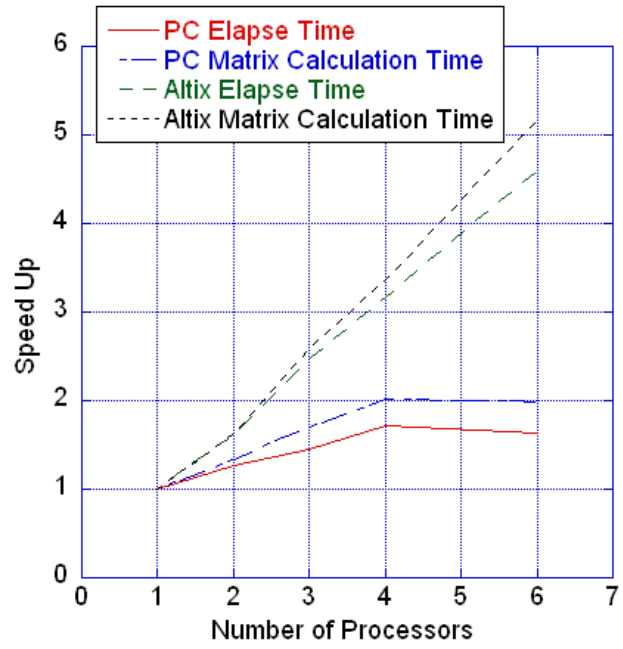

Fig.19 Speed up of parallel computations: comparison between parallel computer and PC cluster.

time consuming part, and the Bi-CGSTAB method is parallelized in our simulations. The data communication is, however, necessary for each iteration step. It is shown in Figs. 18 and 19 that the data communication rate is important and critical for the parallel calculation of the pressure Poisson equations.

4 Conclusion

Three-dimensional shape oscillations of a rotating liquid droplet have been simulated numerically using the level set method, and the combined effects of amplitude and rotation on the oscillation frequency was studied. It was shown that the oscillation frequency decreased as the oscillation amplitude increased, while it increased as the rotation rate increased. The pressure difference between the top and the side of the droplet corresponded to the frequency shift. The oscillations without frequency shift and pressure difference were possible by an appropriate combination between the amplitude and the rotation rate. It was found that the relation between the amplitude and the rotation rate was linear both for the frequency shift of zero and for the pressure difference of zero even though the fluid properties were different. The flow fields in and around the droplet have been visualized, and it was shown that the vortices, which were formed by the shape oscillation, were not much affected by the rotation. The calculation of pressure Poisson equation using the Bi-CGSTAB method has been parallelized. The parallel efficiency was satisfactory, and the importance of the communication rate was demonstrated. Our approach using the parallel level set method would be an accurate and efficient simulation method for simulations of complicated fluid phenomena involving two-phase interfaces [19] or free surfaces [20,21].

References:

[1] V. Shatrov, J. Priede and G. Gerbeth, Three-dimensional linear stability analysis of the flow in a liquid spherical droplet driven by an alternating magnetic field, *Phys. Fluid*, Vol. 15, 2003, pp. 668-678.

[2] W. K. Rhim and S. K. Chung, Isolation of crystallizing droplets by electrostatic levitation, *Methods:A Companion to Methods in Enzymology*, Vol. 1, 1990, pp. 118-127.

[3] A. L. Yarin, D. A. Weiss, G. Brenn, and D. Rensink, Acoustically levitated drops: drop oscillation and break-up driven by ultrasound modulation, *J. Multiphase Flow*, Vol. 28, 2002, pp. 887-910.

[4] H. Lamb, *Hydrodynamics*, Cambridge University Press, 1932.

[5] E. Trinh and T. G. Wang, Large-amplitude free and driven drop-shape oscillations: experimental

observations, *J. Fluid Mech*, Vol. 122, 1982, pp. 315-338.

[6] J. A. Tsamopoulos and R. A. Brown, Nonlinear oscillations of inviscid drops and bubbles, *J. Fluid Mech*, Vol. 127, 1983, pp. 519-537.

[7] H. Azuma and S. Yoshihara, Three-dimensional large-amplitude drop oscillations: experiments and theoretical analysis, *J. Fluid Mech.*, Vol. 393, 1999, pp. 309-332.

[8] F. H. Busse, Oscillation of a rotating liquid drop, *J. Fluid Mech.*, Vol. 142, 1984, pp. 1-8.

[9] C. P. Lee, M. J. Lyell and T. G. Wang, Viscous damping of the oscillations of a rotating simple drop, *Phys. Fluid*, Vol. 28, 1985, pp. 3187-3188.

[10] T. G. Wang, A. V. Anilkumar, C. P. Lee and K. C. Lin, Bifurcation of rotating liquid drops: results from USML-1 experiments in space, *J. Fluid Mech.*, Vol. 276, 1994, pp. 389-403.

[11] M. Sussman and P. Smereka, Axisymmetric free boundary problems, *J. Fluid Mech.*, Vol. 341, 1997, pp. 269-294.

[12] Y. C. Chang, T. Y. Hou, B. Merriman and S. Osher, A level set formulation of Eulerian interface capturing methods for incompressible fluid flows, *J. Comp. Phys*, Vol. 142, 1996, pp. 449-464.

[13] A. A. Amsden and F. H. Harlow, A simplified MAC technique for incompressible fluid flow calculations, *J. Comp. Phys.*, Vol 6, 1970, pp. 322-325.

[14] M. Benzi, Preconditioning techniques for large linear systems: a survey, *J. Comp. Phys.*, Vol. 182, 2002, pp. 418-477.

[15] M. Sussman, P. Smereka and S. Osher, A level set approach for computing solutions to incompressible two-phase flow, *J. Comp. Phys.*, Vol. 114, 1994, pp. 146-159.

[16] T. Watanabe, Numerical simulation of oscillations and rotations of a free liquid droplet using the level set method, *Computers & Fluids*, Vol. 37, 2008, 91-98.

[17] P. Annamalai, E. Trinh, and T. G. Wang, Experimental study of the oscillations of a rotating drop, *J. Fluid Mech*., Vol. 158, 1985, pp. 317-327.

[18] T. Watanabe, Zero frequency shift of an oscillating-rotating liquid droplet, *Phys. Lett. A*, Vol. 372, 2008, pp. 482-485.

[19] N. M. S. Hassan, M. M. K. Khan and M. G. Rasul, Characteristics of air bubble rising in low concentration polymer solutions, *WSEAS Trans. Fluid Mech.*, Vol. 2, 2007, pp. 53-60.

[20] M. DeMarchis and E. Napoli, 3D Numerical simulation of curved open channel flows, *WSEAS Trans. Fluid Mech.*, Vol. 1, 2006, pp. 175-180.

[21] L. A. Mironova, O. I. Gubanov and S Kocabiyik, Numerical simulation of flow past an oscillating cylinder close to a free surface, *WSEAS Trans. Fluid Mech.*, Vol 1, 2006, pp. 297-303.